https://doi.org/10.5194/egusphere-2026-4744
Preprint. Discussion started: 21 August 2026


# Are mesoscale eddies enclosed deserts or productive oases? Satellite-derived evidence of chlorophyll depletion in eddy cores of the southeastern Mediterranean Sea

Merav Gilboa[1,2], Ayah Lazar[1], Ilana Berman-Frank[2], Tamar Guy-Haim[1,3]

[1]National Institute of Oceanography, Israel Oceanographic and Limnological Research, Haifa 3102201, Israel
[2]Department of Marine Biology, Leon H. Charney School of Marine Sciences, University of Haifa, Haifa 3103301, Israel
[3]Department of Life Sciences, Ben-Gurion University of the Negev, Beer Sheva 84105, Israel

*Correspondence to*: Merav Gilboa (Mrvgilboa@gmail.com); Tamar Guy-Haim (tamar.guy-haim@ocean.org.il)

**Abstract.**
Mesoscale eddies are fundamental drivers of physical and biological variability in the ultra-oligotrophic Southeastern Mediterranean Sea (SEMS). By integrating two long-term satellite altimetry datasets (DYNED and PET, 1993–2025), this study characterizes the seasonal spatiotemporal dynamics of cyclonic (CE) and anticyclonic (ACE) eddies and assesses their ecological impacts on phytoplankton biomass. Our analysis reveals polarity-based dynamics, though several physical metrics are sensitive to eddy-detection method: ACEs showed a tendency toward longer lifetimes than CEs, rotational velocity rankings reversed between datasets, and CEs consistently dominated high-density spatial hotspots. Seasonal patterns indicate peak eddy activity between February and April, followed by a basin-wide decline during the summer months. Our investigation of surface chlorophyll-a (Chl *a*) distributions challenges the classical "productive oasis" paradigms; most CEs demonstrate negative Chl *a* anomalies and depleted cores, potentially driven by intense top-down grazing pressure. Conversely, ACEs encompass larger areas of influence and may therefore facilitate greater horizontal retention, producing a larger area-integrated surface Chl *a* footprint and potentially supporting greater phytoplankton biomass through bottom-up nutrient accumulation. Our findings suggest that mesoscale features in the SEMS function as active ecological mechanisms, restructuring the basal food web via differential transport, retention, and community succession. This work emphasizes the need for coupled physical-biological frameworks to understand ecosystem resilience in nutrient-impoverished basins facing global climate change.

## 1 Introduction

The circulation of the Eastern Mediterranean Sea is complex and influenced by the large-scale counterclockwise circulation around the basin and by regional variability, associated with intermittent eddies and jets. These features are modulated by external climate influences and oscillatory systems, such as the Adriatic-Ionian Bimodal Oscillation System (Eusebi Borzelli and Carniel, 2023; Gačić et al., 2013;

https://doi.org/10.5194/egusphere-2026-4744
Preprint. Discussion started: 21 August 2026


Ozer et al., 2022). Mesoscale eddies, rotating bodies of water spanning tens to hundreds of kilometers, play an important role in shaping the ocean's physical, chemical, and biological environment. These structures with separate polarities; cyclonic (CE) and anticyclonic (ACE), influence marine ecosystems by redistributing heat, salt, nutrients, and planktonic organisms (Condie and Condie, 2016). Characterizing the temporal dynamics, area of influence (AOI), and occurrence of these eddies is critical, especially in semi-enclosed basins like the Mediterranean, where mesoscale activity has significant impacts on biological productivity and connectivity (Belkin et al., 2022). A deeper look into seasonal patterns and spatial variation can provide insight into the influence of physical mesoscale structures on pelagic ecosystems.

Long-term eddy datasets have improved our understanding of mesoscale variability by enabling analyses of eddy occurrence, trajectories, and long-term variability. Previous studies have also shown that eddy characteristics may depend on the detection method; for example, standard altimetry products tend to overestimate the size of cyclonic eddies relative to anticyclonic eddies (Mkhinini et al., 2014). In the southeastern Mediterranean Sea (SEMS), Barboni et al. (2021) further showed that the Eratosthenes Seamount acts as an attractor for anticyclonic eddies in the SEMS, with many of these features eventually merging with the semi-permanent Cyprus Eddy, located over the Eratosthenes Seamount.

Although mesoscale eddies in the SEMS have been studied and their impacts were recognized, their seasonal dynamics and ecological effects on plankton communities remain poorly understood. Globally, mesoscale eddies are fundamental drivers of marine biogeochemistry that modify surface Chl *a* distributions through mechanisms such as nutrient pumping, lateral advection, and fluid trapping (McGillicuddy, 2016). Cold core cyclonic and warm core anticyclonic eddies have been shown to substantially modify nutrient concentrations and phytoplankton biomass. For example, in the Northwest Pacific, cold eddies can enhance Chl *a* concentrations by up to 134%, whereas warm eddies may reduce dissolved inorganic nitrogen and phosphate by as much as 70% relative to surrounding waters (Kang et al., 2022).

Understanding how eddies affect nutrient dynamics and availability is especially important in the ultraoligotrophic SEMS, where nutrient availability strongly controls primary production. Regionally, the distinct Chl *a* influence of these structures was highlighted by (Tanaka et al., 2007) within the Cyprus eddy. Their work demonstrated how this prominent warm core anticyclone alters the vertical distribution of limiting nutrients, confining peak Chl *a* concentrations to approximately 0.12 mg per cubic meter within a Deep Chlorophyll Maximum (DCM) located between 100 and 130 meters. Crucially, the downwelling physics of this warm core depressed the nutricline, resulting in nutrient and Chl *a* levels that were approximately twice as high in the unperturbed boundary waters outside the eddy compared to its highly depleted core. This sustained distinct microbial food web dynamics within the interior compared to the surrounding environment.

Chl *a* is commonly used as a proxy for phytoplankton biomass and, indirectly, for primary productivity, particularly in oligotrophic systems where Chl *a* responses to physical forcing are often subtle and spatially heterogeneous (Mahadevan, 2014; Volpe et al., 2012). Mesoscale eddies can modify these distributions through a range of physical and Chl *a* mechanisms, including nutrient supply, lateral advection, water mass trapping, changes in mixed layer depth, and retention of planktonic communities within eddy cores or along peripheries (Clayton et al., 2013; Condie and Condie, 2016). Recent global analyses further suggest that mesoscale eddies can trap and transport large amounts of Chl *a*, thereby

https://doi.org/10.5194/egusphere-2026-4744
Preprint. Discussion started: 21 August 2026


redistributing and enhancing concentrations in ocean interiors, away from coastal or boundary source regions (Zhao et al., 2022). The Chl *a* response to mesoscale eddies is unlikely to be uniform across eddy types or seasons. In the SEMS, where strong seasonal stratification and episodic mixing impact the already limited availability of phosphorus and nitrogen and thus regulate phytoplankton dynamics, the timing of eddy formation and persistence is likely to be particularly important (Belkin et al., 2022; Ben Ezra et al., 2021; Fadida et al., 2026). Young eddies may reflect the Chl *a* signature of the water masses from which they formed, whereas mature or long-lived eddies may develop distinct Chl *a* signatures through prolonged retention, nutrient redistribution, and community succession (Condie and Condie, 2016; McGillicuddy, 2016; Zhao et al., 2022). We therefore hypothesize that Chl *a* concentrations and anomalies differ between cyclonic and anticyclonic eddies and vary with both eddy age and season. We further expect the strongest Chl *a* responses when eddy persistence coincides with periods of enhanced nutrient availability or phytoplankton growth.

Understanding the temporal dynamics in terms of occurrence patterns, area of influence, and trajectories of mesoscale eddies is critical, especially in semi-enclosed seas like the Mediterranean, where such features significantly impact Chl *a* productivity and connectivity. Here, we aimed to: (**1**) quantify seasonal occurrence, trajectories, and areas of influence of cyclonic and anticyclonic eddies in the SEMS; (**2**) examine how surface Chl *a* varies with eddy polarity, age and season; and (**3**) discuss the potential ecological implication, knowledge gaps, and methodological limitations. To address these objectives, we combined two long-term eddy atlases, DYNED and the Py Eddy Tracker (PET) with satellite-derived Chl *a* observations. We analyzed eddy lifetimes, areas of influence, occurrence patterns, and trajectories to characterize the spatiotemporal variability of mesoscale eddies in the SEMS and examine their relationship with surface Chl *a* as an indicator of potential ecological effects.

## 2 Methods

### 2.1 Datasets

This study focused on the Southeastern Mediterranean Sea, specifically the region between 31°N–34.5°N and 32°E–36°E, encompassing the Levantine Basin adjacent to the coasts of Israel and Lebanon, limited by Cyprus to the west and north (following Barboni et al., 2023). Two eddy atlases were used in this study: the DYNED Atlas (2000-01-02 to 2017-12-06) and the Py Eddy Tracker (PET) Atlas. Both datasets provide daily trajectories at a spatial resolution of 0.25×0.25°. The PET Atlas consists of two complementary products: the PET Historical dataset (1993-01-01 to 2021-12-31) and the PET NRT dataset (2018-01-01 to 2025-05-19). PET Historical dataset uses reprocessed (multi-year) altimetry data, incorporating all available satellite missions with precise orbit corrections and cross-calibration. In contrast, PET NRT uses near real-time altimetry, processed usually within 24 hours using preliminary orbits. These files may contain minor errors corrected in the reprocessed versions. The DYNED Atlas combines eddies detected from satellite altimetry using the Angular Momentum Eddy Detection Algorithm (AMEDA) with associated Argo float observations (Barboni et al., 2021; Stegner and Le Vu, 2022).

https://doi.org/10.5194/egusphere-2026-4744
Preprint. Discussion started: 21 August 2026


The additional analysis was performed on the Eddy-trajectory Meta3.2 NRT (Aviso) Atlas based on the Py-eddy-Tracker algorithm (Mason et al., 2014), which supplied comparable statistical analysis for a more recent period (2020-2025). AMEDA identifies eddies from sea surface height anomalies, vorticity, and velocity fields by locating closed streamlines that define eddy boundaries. Eddies are then tracked through time based on their centers and boundaries, allowing the estimation of eddy lifetime (duration before dissipation or merging) and maximum azimuthal velocity.
The Eddy Trajectory Atlas META3.2 NRT is based on the Py-Eddy-Tracker (PET) algorithm (Mason et al., 2014). PET identifies eddies from high-pass filtered Absolute Dynamic Topography (ADT), locating local extrema surrounded by their initial closed contours, which must subsequently satisfy strict criteria for shape circularity (< 70\% error) and minimum sea surface height anomaly amplitude (> 0.4 cm). The principal differences between the AMEDA and PET detection algorithms are summarized in Table 1.

**Table 1**. Comparison of parameters used in the AMEDA and PET algorithms for eddy detection.

| Parameter | AMEDA (Le Vu et al. 2018) | Py-eddy-tracker (Pegliasco et al., 2022) |
|---|---|---|
| Primary Method | Hybrid: Geometrical (streamlines) + Dynamical (velocity). | Geometrical: Scanning closed ADT/SLA contours. |
| Detection Center | Local extrema of LNAM. | Local extrema of SSH (minima for cyclones, maxima for anticyclones). |
| Contour Interval | Based on velocity streamlines. | Scans contours between -100 to 100 cm with a 0.2 cm interval. |
| Shape Constraint | Uses ellipticity and steepness of the velocity profile. | Shape error ≤ 70% (deviation from a circle). |
| Size Constraint | Minimum radius is often set (~30-40 km). | Pixel-based: 5 ≤ Npixel ≤ 1000. |
| Amplitude | Not a primary filter for detection. | Amplitude ≥ 0.4 cm (to avoid noise). |

## 2.2 Eddy areas of influence and trajectories

The measurement of the AOIs (areas of influence) was done by calculating the convex hull of eddies along their trajectories over their lifetimes, representing the cumulative surface footprint based on detected positions and radii. For each time step, the eddy center was buffered using the corresponding eddy radius, producing a sequence of circular influence areas along the trajectory. These time-step buffers were then merged, and a convex hull was calculated to represent the total AOI of each eddy over its lifetime.
To quantify spatial overlap among eddies, individual AOI geometries were overlaid, and the density of overlapping geometries was calculated across the study region. This provided a spatial estimate of areas repeatedly influenced by eddies during the analysed period. Eddy occurrence was defined as the density of eddies detected with a specified period, or throughout the full dataset if the period was unspecified.

https://doi.org/10.5194/egusphere-2026-4744
Preprint. Discussion started: 21 August 2026


Spatial analyses were performed in Python using pandas and Shapely. Eddy trajectories were analyzed using the Moving Pandas module (Graser and Dragaschnig, 2020), a python package integrated into pandas and geopandas to analyse movement and trajectories, performing tasks such as smoothing, generalization, clustering and filtering. Sensitivity tests were done to obtain the optimised generalization for Eddy trajectories using the Douglas-Peucker algorithm at E = 0.1 degrees using a long Trajectory number 6039 (2009-05-20 00:00:00 to 2009-12-21 00:00:00), Size: 200 days, Length: 874125.1 m.

### 2.3 Chlorophyll-a

Surface Chl *a* concentration data was downloaded from the Copernicus Datastore, the daily Chl *a* variable med-ogs-pft-rean-d was used from product ID: MEDSEA_MULTIYEAR_BGC_006_008 (Teruzzi et al., 2021). All Chl *a* analyses were based exclusively on eddies identified in the DYNED Atlas, thereby ensuring methodological consistency and avoiding confounding effects associated with combining different eddy products. For each eddy, mean and integrated surface Chl *a* concentrations were calculated using the location and date of the eddy center derived from the DYNED Atlas, at the time step when azimuthal velocity was maximal.

Mean Chl *a* is calculated as the average spatial concentration of Chl *a* at the sea surface within the eddy's defined boundary. The surface area of the eddy used for estimating mean surface Chl *a* was defined using the reported mean radius:

$$(1)\ Chl_{mean} = \frac{1}{N} \sum C_i\ ;$$

where Ci is the Chl *a* concentration at pixel i, and N is the total number of pixels contained within the eddy buffer area.

Integrated surface Chl *a* values were obtained by summing all raster cell values within the eddy area:

$$(2)\ Chl_{int} = Chl_{mean} \times A_i\ :$$

where $A_i$ is the area (in m²) of the buffered geometry calculated using a projected coordinate system (e.g., EPSG:2039).

### 2.4 Comparative analysis of inter- and intra- eddy Chl *a* concentrations

To quantify the Chl *a* influence exerted by mesoscale features, we adopted the methodology similar to Cael et al.(Cael et al., 2026) evaluating the divergence between Chl *a* concentrations within the eddy core ($Chl_{in}$) and the ambient background environment ($Chl_{out}$).

*Spatial characterization*:

Internal (core) domain: This region was delineated by the area enclosed within the maximum speed contour or the defined buffered radius (R).

Effective or speed contour (margin) domain: This was defined as mean surface Chl *a* values along the points of the polygon for the contour shape of each feature.

External (background) domain: This was defined as a concentric annular ring extending from 1.5×R to 2.5×R. Such a configuration ensures that the reference water mass is geographically proximal while remaining outside the immediate physical sphere of the eddy's influence.

A visual representation of the spatial characterization scheme is illustrated in Fig. A1.

*Analytical metrics:*

https://doi.org/10.5194/egusphere-2026-4744
Preprint. Discussion started: 21 August 2026


Chl *a* anomaly (ΔChl): Computed as the difference between internal pigment levels and the reference background values:

$$\Delta Chl = Chl_{in} - Chl_{out} \quad (3)$$

### 2.5 Statistical analyses

Statistical analyses were conducted in Python utilizing the *SciPy, Statsmodels*, and *scikit-posthocs* libraries to evaluate mesoscale eddy dynamics and their corresponding Chl *a* signatures. For each eddy characteristic, differences between cyclonic (CE) and anticyclonic (ACE) eddies were assessed separately within the DYNED and PET datasets using two-sided Mann–Whitney U tests. To assess variance across categorical groupings (e.g., eddy polarity, seasonal bins, and life stages), parametric Analysis of Variance (ANOVA) and Welch's independent t-test were applied when assumptions of normality were met. For nonparametric distributions, the Kruskal-Wallis H test was employed, followed by Dunn's post-hoc test to isolate specific group-level divergences. Structural modality, multimodality in parameters such as monthly eddy occurrences and Chl *a* concentration, was evaluated using Hartigans' dip test, where a significant p-value indicates evidence against unimodality. Linear dependencies between continuous variables, such as maximum rotational velocity and mean or integrated Chl *a* concentrations, were quantified using Pearson correlation coefficients. For temporal dynamics, Fast Fourier Transform (FFT) spectral analysis was applied to continuous time series data (unique daily and annual eddy counts) to identify dominant periodicities. Furthermore, cross correlation and frequency domain coherence models were utilized to examine the temporal relationship between rotational speed and Chl *a* concentration along individual continuous eddy tracks. A significance threshold of $\alpha$=0.05 was applied across all statistical testing. Visualizations accompanying these analyses, including scatter plots, boxplots, violin plots, line plots, and histograms, were generated primarily using *cartopy*, *matplotlib* and *seaborn* packages.

## 3 Results

### 3.1 Eddy characteristics

Mesoscale eddy dynamics in the Levantine Basin exhibited distinct physical and statistical signatures across the DYNED (2000–2017) and PET Historical (1993–2021) datasets. Statistical comparisons between polarities (ACE vs. CE) revealed product-specific sensitivities in detection and tracking metrics. Within the geographic area of the SEMS, 295 anticyclonic eddies (ACEs) and 200 cyclonic eddies (CEs) have been detected using AMEDA, and recorded in the DYNED Atlas, while long-term PET data detected 760 CEs and 441 ACEs. Analysis of the DYNED Atlas indicates that ACEs generally persisted longer than CEs, with mean lifetimes of 95 and 85 days (Fig 1a), respectively, although this polarity-based variation lacks statistical significance ($p = 0.053$). The PET Historical dataset records substantially shorter durations for both features (Fig 1a, ACE = 44 days; CE = 34 days), showing no statistically significant divergence between the two types ($p = 0.49$). The distinct structural criteria separated DYNED and PET products. Within the DYNED dataset, features appeared more compact, yet ACEs maintained a significantly greater mean radius (27 km) compared to CEs (23 km; $p < 0.001$, Fig 1c). In contrast, the

https://doi.org/10.5194/egusphere-2026-4744
Preprint. Discussion started: 21 August 2026


PET Historical atlas identified broader mesoscale structures, where CEs exhibited a slightly larger radial extent (41 km) than their anticyclonic counterparts (38 km; $p < 0.001$). Rotational velocity revealed diverging trends across the products. Within the DYNED Atlas, cyclonic features exhibited a significantly greater mean velocity (12 cm $s^{-1}$) relative to anticyclonic structures (10 cm $s^{-1}$; p = 0.019) while the PET Historical record indicated ACEs maintain higher rotational intensities (12 cm $s^{-1}$) compared to their cyclonic counterparts (11 cm $s^{-1}$; $p < 0.001$, Fig 1d). Total displacement distances revealed that DYNED ACEs traversed significantly greater distances (135 km) relative to CEs (97 km; $p < 0.001$). In contrast, the PET Historical dataset showed more constrained mean trajectories, averaging 41 km for anticyclonic and 45 km for cyclonic features ($p = 0.0092$, Fig 1b). To ensure population comparability and focus on typical mesoscale activity, these physical distributions excluded exceptionally persistent anomalies with lifetimes exceeding 400 days.

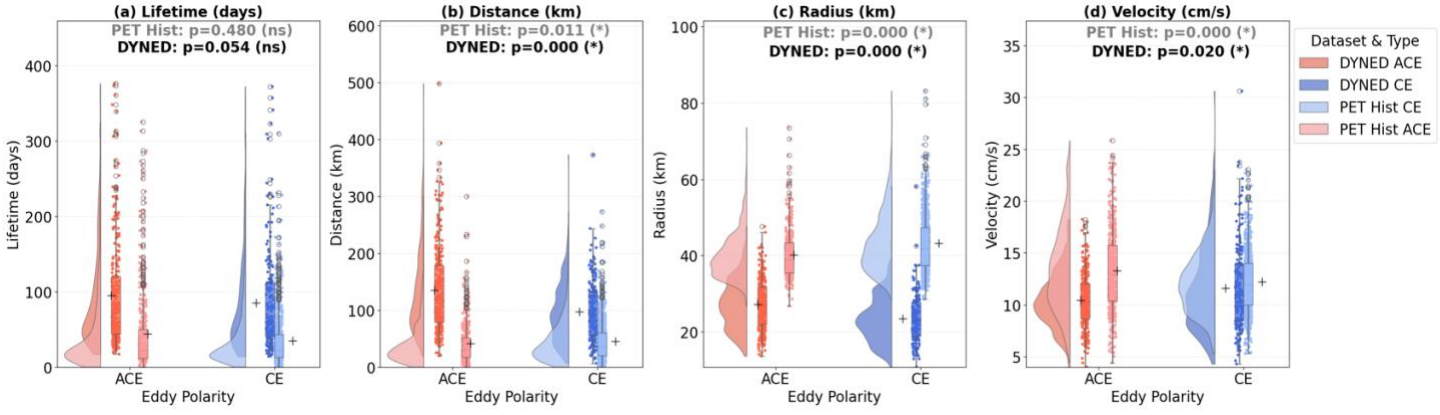


**Figure 1**. Comparative analysis of physical eddy properties between the DYNED and PET datasets. Raincloud plots illustrate the probability density and distribution of four fundamental metrics: (**a**) Lifetime (days), (**b**) Total displacement distance (km), (**c**) Mean radius (km), and (**d**) Maximum azimuthal velocity (cm $s^{-1}$). Features are differentiated by polarity: anticyclonic (ACE, red) and cyclonic (CE, blue), and data source, where solid and shaded regions correspond to the DYNED Atlas and PET Historical dataset, respectively. The visualization includes split-violin plots, raw data points, and standard boxplots representing median values and interquartile ranges, while mean values are indicated by crosses (+). To maintain population comparability, only eddies with lifetimes under 400 days are included. Subplots include source-specific p-values from Mann-Whitney U tests.

### 3.2 Temporal variability of eddies

Periods of intensified eddy activity, particularly for ACEs, from 2010 to 2014 were apparent (Fig. 2a) although no significant trend in annual occurrences was detected. Spectral analysis indicated a dominant cycle of approximately 3.6 years with a power of 1.87 for the annual occurrence of anticyclonic eddies, and a longer dominant cycle of around 9.0 years with a power of 2.94 for cyclonic eddies. Eddies in the SEMS displayed a variable annual pattern (Fig. 2b), with enhanced activity during specific months, particularly among ACEs. Eddy occurrences peaked between February and April and strongly declined during the summer months of May to July, while intensified again from August to November.

https://doi.org/10.5194/egusphere-2026-4744
Preprint. Discussion started: 21 August 2026


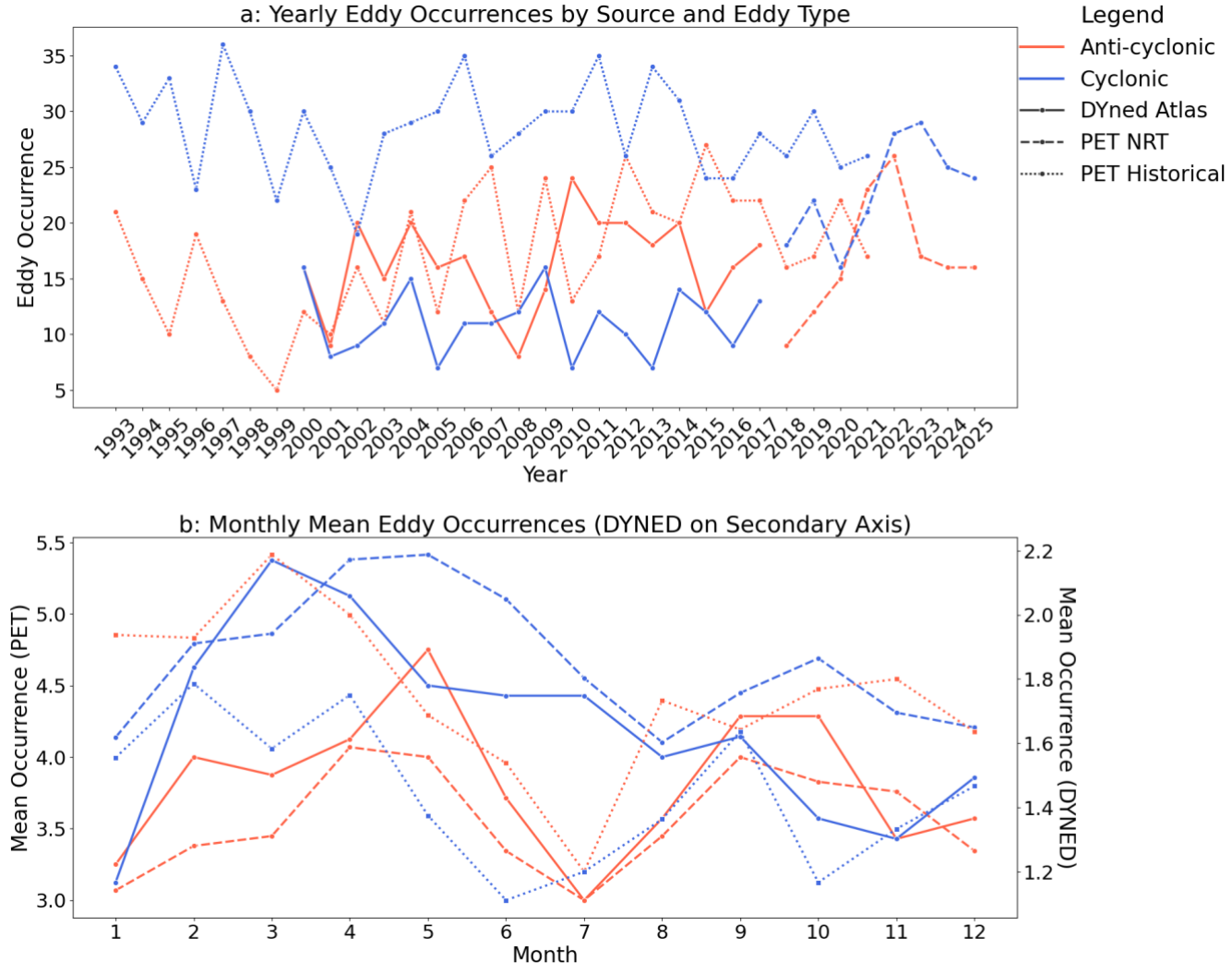


**Figure 2**. Comparative analysis of temporal eddy dynamics across multiple atlases. This visualization illustrates the longitudinal and seasonal trends of mesoscale features in the Southeastern Levantine Basin, integrating data from the DYNED Atlas, Copernicus PET NRT, and PET Historical datasets. (**a**) Yearly Eddy Occurrences: Total annual count of unique trajectories, highlighting inter-annual variability and differences in detection magnitude across altimetric products. (**b**) Monthly mean eddy occurrences: Climatological seasonal patterns representing the mean number of active tracks per month for each time series. Anticyclonic [ACE], red; Cyclonic [CE], blue, data sources indicated by distinct markers and line styles.

Within the PET Historical dataset, mean monthly occurrence reached an annual maximum of 4.8–5.4 active tracks between February and April, while the DYNED Atlas showed a concurrent but lower peak of 2.2 active tracks per month. Following this early-spring maximum, eddy occurrence declined sharply from May to July, reaching a minimum in July across all datasets. Mean monthly occurrence decreased to approximately 3 active tracks in PET and 1.1 active tracks in DYNED. Eddy activity subsequently

https://doi.org/10.5194/egusphere-2026-4744
Preprint. Discussion started: 21 August 2026


increased during late summer and autumn, forming a secondary seasonal peak between August and November. This autumn intensification reached maxima of 4.7 active tracks per month in PET in October and 1.8 active tracks per month in DYNED in September.

### 3.3 Seasonal and spatial chlorophyll patterns within eddies

Surface Chl *a* concentration in the basin were governed by a dominant seasonal cycle, transitioning from intensified late winter and early spring blooms to a state of extreme low Chl *a* values during the summer months (Fig. 3, $\leq$0.025 mg $m^{-3}$).

Chl *a* concentration in both CEs and ACEs exhibited clear seasonal patterns, with differences observed between the eddy types (Fig. 4). Mean Chl *a* (mg $m^{-3}$) was consistently higher in CEs, peaking at approximately 0.14 mg $m^{-3}$ in December, compared to ACEs, which reach a lower peak of about 0.07 mg $m^{-3}$ in May. Both eddy types follow a non-unimodal seasonal trend for mean Chl *a*, showing maxima in spring and late autumn/early winter, and minima during winter and summer. CEs also displayed greater variability in mean Chl *a*.

In contrast, integrated Chl *a* (mg $m^{-1}$) was generally higher in ACEs, which peak around 670 mg $m^{-1}$ in May-June. CEs show a lower integrated Chl *a* maximum of about 430 mg $m^{-1}$ during the same period. Like mean Chl *a*, integrated Chl *a* for both eddy types also followed a bimodal seasonal cycle, with peaks in spring and autumn and troughs in winter and summer. ACEs consistently demonstrated a wider range of integrated Chl *a* value. The observed intra-annual Chl *a* signal synchronized with increased occurrences phases identified in temporal cycles. Welch's t-tests confirm that significant Chl *a* divergence between anticyclonic and cyclonic populations is concentrated during the transitional windows of June, July, October and December ($p < 0.05$) for mean concentrations, while a marked divergence in integrated Chl *a* occurs in November. Integrated concentrations within ACEs peaked in May and June, approaching statistically significant differences from CEs ($p \approx 0.055$, $p \approx 0.064$, respectively).

https://doi.org/10.5194/egusphere-2026-4744
Preprint. Discussion started: 21 August 2026


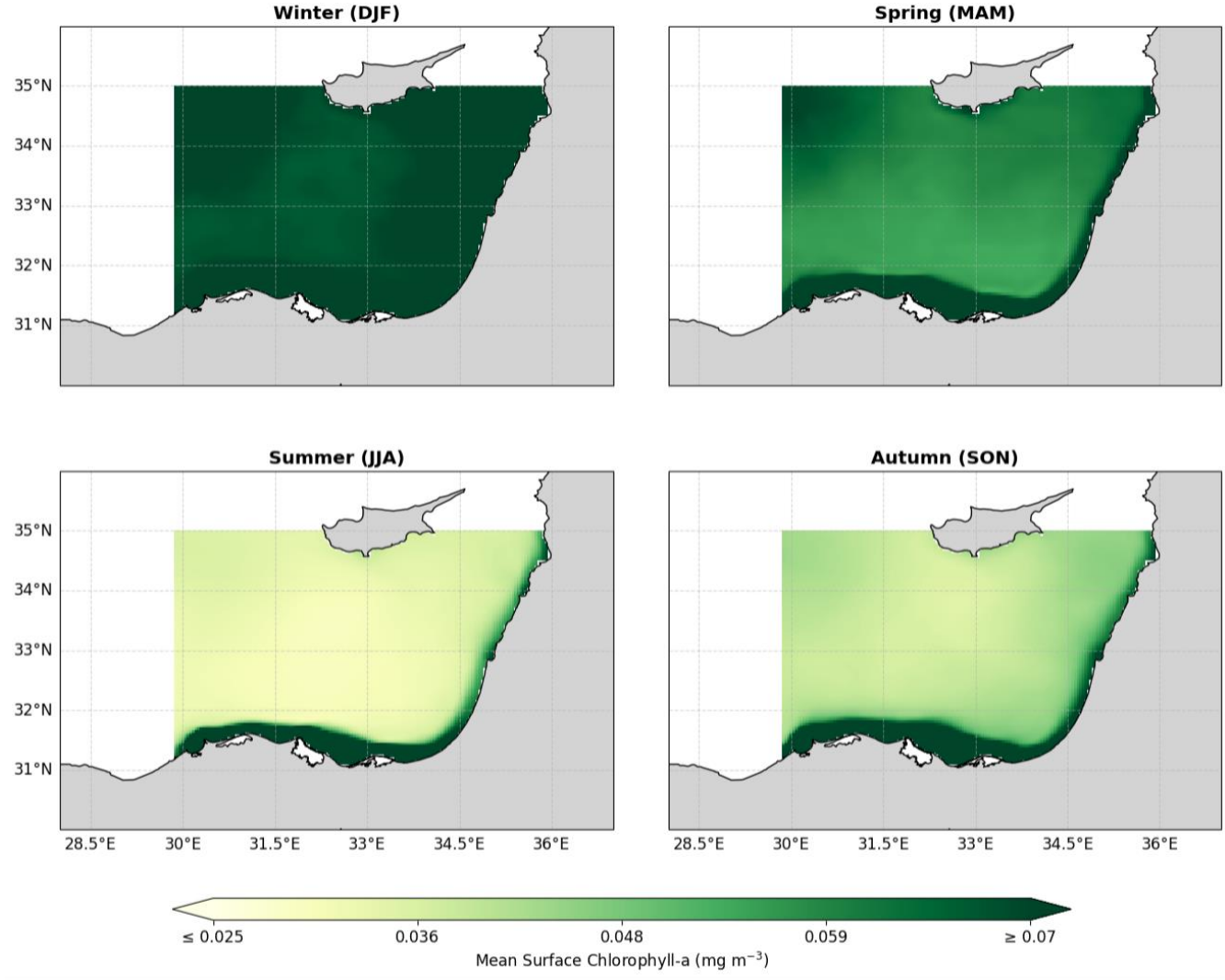


**Figure 3**. Seasonal baseline surface Chl *a* concentrations in the Southeastern Levantine Basin. This figure illustrates the mean monthly surface Chl *a* levels (mg $m^{-3}$) across the study area for the study time period using the data product MEDSEA_MULTIYEAR_BGC_006_008 (Teruzzi et al., 2021), highlighting seasonal fluctuations and peak conditions.

The spatial variability of surface Chl *a* across these mesoscale features exhibited a complex radial gradient, diverging from traditional core-centered productivity models. Global Kruskal-Wallis analysis revealed highly significant spatial heterogeneity among the four delineated domains (Fig. 5): the core, effective margin, speed margin, and outer ring; $H = 6094.58$, $p < 0.001$). Dunn post hoc test further demonstrated that Chl *a* signatures between anticyclonic and cyclonic populations differed significantly across all zones, including the core and background environment. For CEs, average core Chl *a* concentrations were 0.0542 mg $m^{-3}$. Statistical testing quantitatively identified an inverse doming effect

https://doi.org/10.5194/egusphere-2026-4744
Preprint. Discussion started: 21 August 2026


within CEs: core pigment levels were 5.11% lower than those in the surrounding speed margin (0.0571 mg $m^{-3}$). Simultaneously, this core concentration reflected a notable 32.22% Chl *a* deficit compared to the proximal ambient outer ring (0.0800 mg $m^{-3}$; $p < 0.001$). Hartigans' dip test ($p < 0.001$) suggests that Chl *a* distributions within the core and outer ring were statistically not unimodal, indicating that CEs encompass a mixture of distinct regimes.

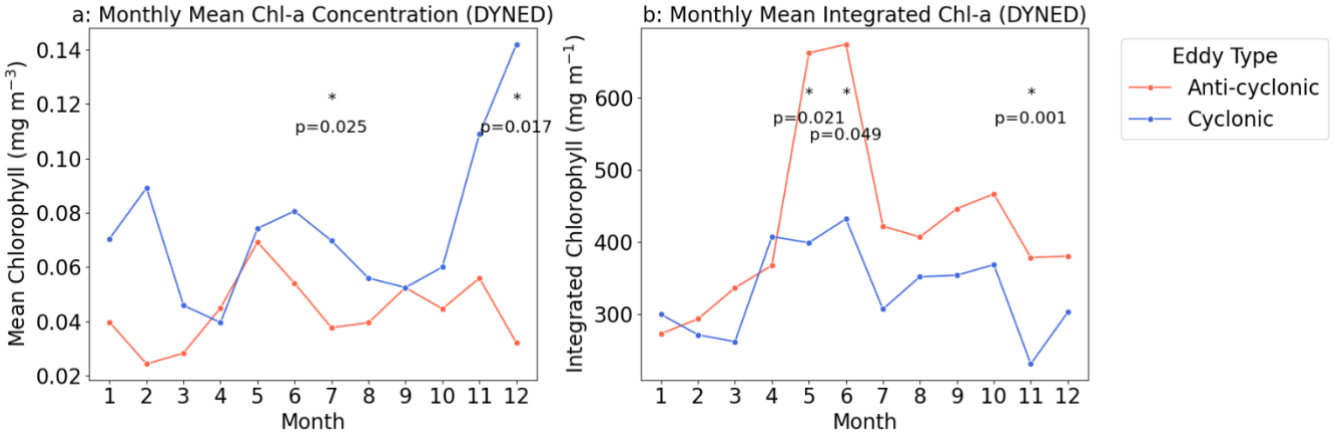


**Figure 4**. Seasonal Chl *a* dynamics within Southeastern Levantine Basin eddies. This multi-panel analysis depicts the monthly Chl *a* signatures associated with mesoscale features between 2000 and 2017. (**a**) Monthly mean Chl *a* concentration: Average surface pigment levels (mg $m^{-3}$) derived from the buffered AOIs of detected eddies, showing peak bloom conditions during the early spring period. (**b**) Monthly Mean Integrated Chl *a*: Total Chl *a* signal summed across the eddy extent, representing the synergistic effect of feature area and Chl *a* magnitude. Data are categorized by polarity (Anticyclonic [ACE], red; Cyclonic [CE], blue). Statistical significance in the Chl *a* divergence between ACEs and CEs is indicated by asterisks (*), representing months where $p < 0.05$ as determined by Welch's t-tests.

https://doi.org/10.5194/egusphere-2026-4744
Preprint. Discussion started: 21 August 2026


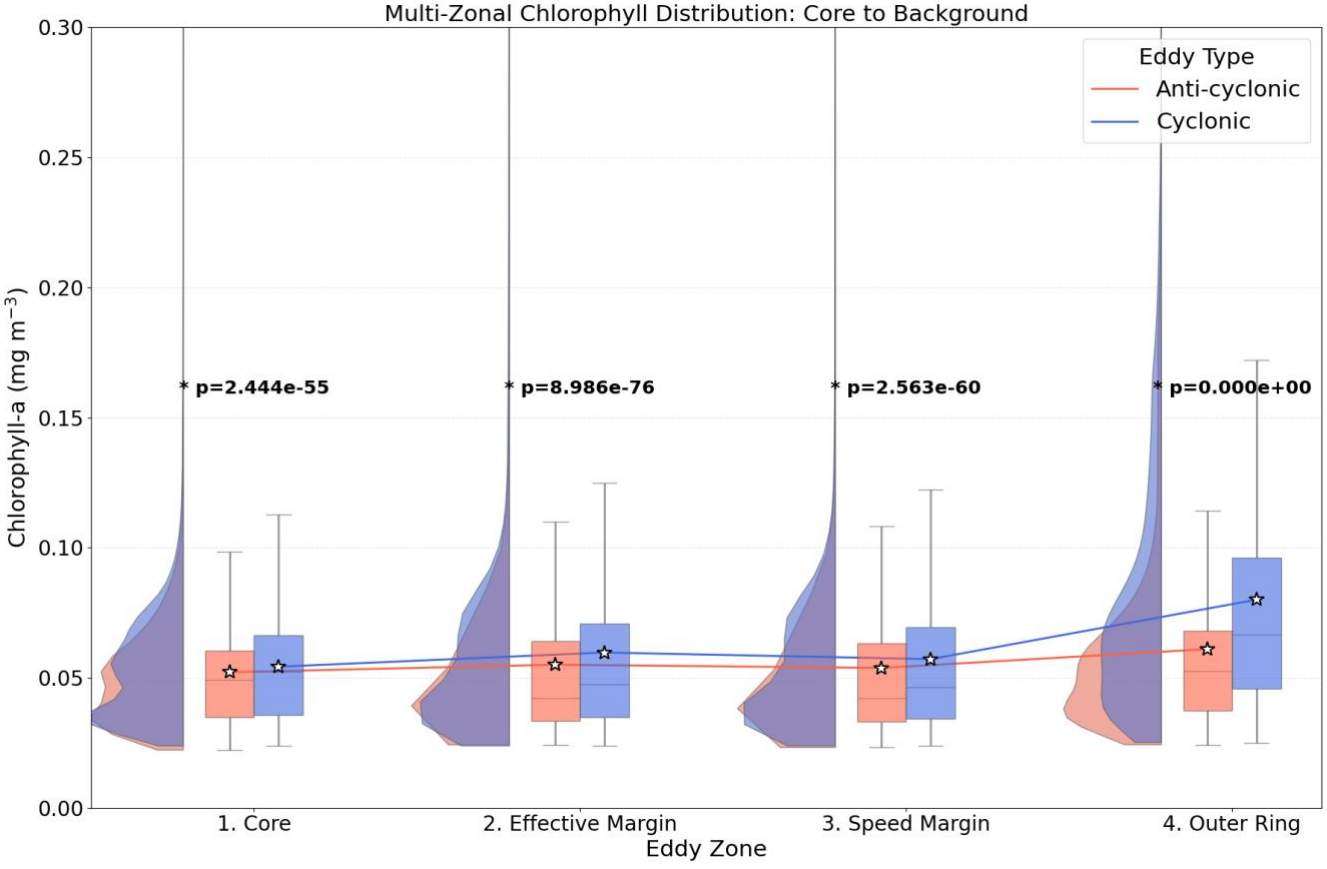


**Figure 5**. Spatial gradient of Chl *a* from the eddy core to background. This raincloud plot illustrates the distribution of mean (stars) surface Chl *a* (mg $m^{-3}$) across four distinct spatial zones: (**1**) the core, (**2**) the effective margin, (**3**) the speed margin, and (**4**) the outer ring (background). The visualization contrasts the surface Chl *a* of anticyclonic (ACE; red) and cyclonic (CE; blue) eddies. Each panel combines a half-violin plot (probability density) and a boxplot (median and interquartile range). To maintain focus on the representative data distribution and mitigate the influence of extreme outliers, the y-axis is capped 0.3 mg $m^{-3}$.

Across both polarities, 77.23% of anomalies in Chl *a* were negative, 80.14% of CEs had negative anomalies and 74.34% of ACEs. Three-way Analysis of Variance (ANOVA) demonstrates that Chl *a* anomaly variability is modulated by synergistic multi-variable interactions. Highly significant drivers include eddy polarity ($F = 43333.52$, $p < 0.001$, $\eta^2 = 0.00041$), seasonal periodicity ($F = 1364.97$, $p < 0.001$, $\eta^2 = 0$), and lifetime stage ($F = 330.61$, $p < 0.001$, $\eta^2 = 0.0001$), with robust interaction across all configurations. Specifically, the statistical interaction models confirm that winter (DJF) is the primary season where ACEs undergo a dramatic, isolated surge in positive Chl *a* anomalies. CEs achieve their highest positive Chl *a* anomalies during autumn (SON; September, October, and November), where internal Chl *a* concentrations spike. The observed intra-annual Chl *a* signals synchronized with physical intensification phases identified in temporal cycles. Cross-correlation analysis reveals a coherent, near-instantaneous anti-phase relationship with zero-day lag, suggesting rapid Chl *a* responses to mesoscale

https://doi.org/10.5194/egusphere-2026-4744
Preprint. Discussion started: 21 August 2026


forcing. Welch's t-tests confirm that significant Chl *a* divergence between anticyclonic and cyclonic populations is concentrated during the transitional windows of July and December ($p < 0.05$) for mean concentrations, while a marked divergence in integrated Chl *a* occurs in November. Inter-polarity variations in integrated pigment levels approach statistical significance during May ($p \approx 0.055$) and June ($p \approx 0.064$), though Chl *a* signatures remain relatively uniform across polarities throughout much of the annual cycle. This strong coupling in the frequency domain is further supported by maximum magnitude-squared coherence values exceeding 0.80 at low-frequency periodicities.

### 3.4 Spatial patterns of eddy occurrences

Analysis of altimetric datasets within the SEMS study region indicates a distinct geographical partitioning and the presence of structured spatial corridors for mesoscale structures (Fig. 6). The foundational Mean Dynamic Topography (MDT) across this Levantine domain exhibits values spanning from an absolute minimum of -0.12 m to a peak elevation of +0.22 m. Areal quantification of cumulative tracking layers reveals a structural divergence in the spatial footprints of each polarity. ACEs dominate diffuse, low-density fields (0–20 counts), covering a cumulative surface extent of 148,437 km² compared to 105,692 km² for CEs. At intermediate tracking densities (21–30 counts), both polarities occupy comparable spatial extents (35,598 km² for CEs; 33,528 km² for ACEs). However, within high-density core hotspots (> 31 counts), CEs heavily dominate the basin, maintaining a cumulative footprint of 72,213 km² across the 31–70 count thresholds. Conversely, ACEs contract sharply to 8,481 km² within the 31–60 count range and terminate entirely above 60 counts.

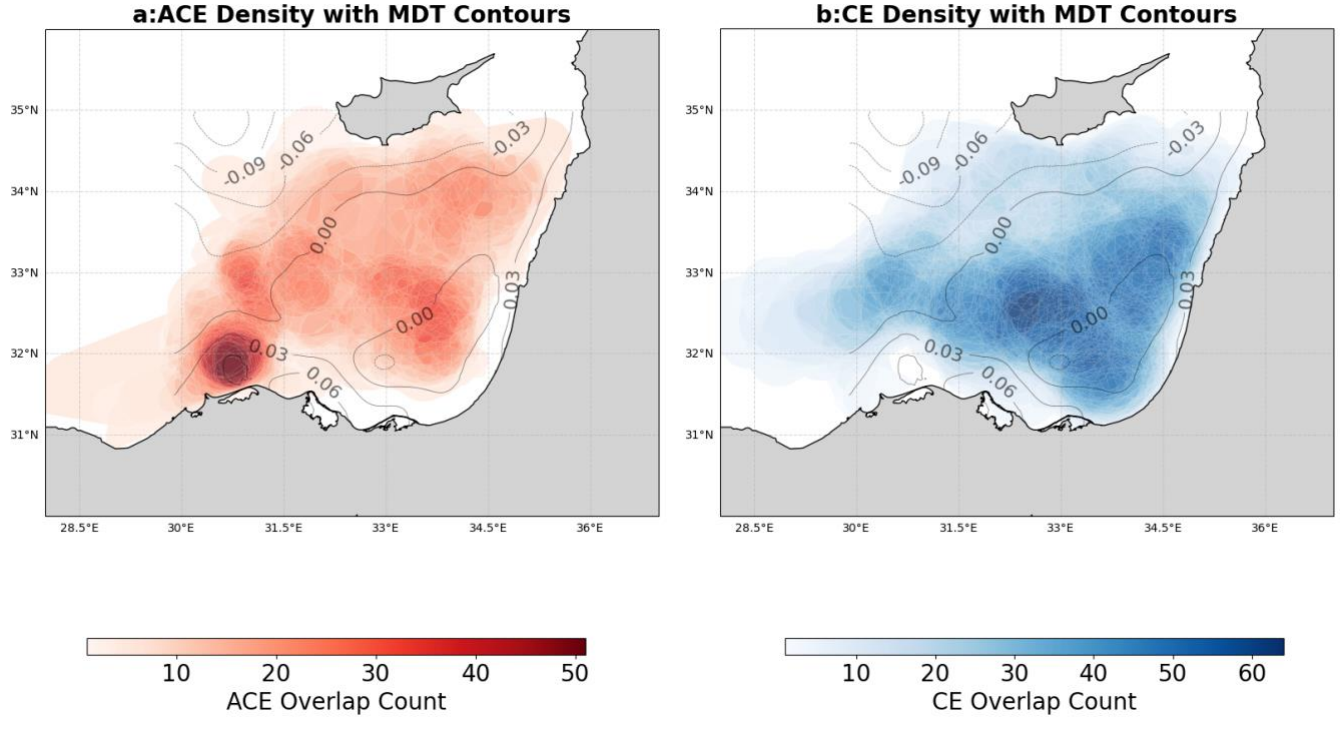

https://doi.org/10.5194/egusphere-2026-4744
Preprint. Discussion started: 21 August 2026


**Figure 6**. Spatial relationship between mean dynamic topography (MDT) and overlaid area of influence (AOI), for anticyclonic (**a**) and cyclonic (**b**) eddies over their lifetime during 2001-2018 in the Southeastern Mediterranean Sea. The area was calculated as a geometric convex hull of eddy trajectories based on their radius at each timestep. This dual-panel visualization illustrates the persistent topographic features of the basin overlaid with regions of high mesoscale eddy occurrence. Discrete black contours (interval labels in meters) represent the MDT.

Seasonal spatial patterns of eddy occurrences and trajectories (Fig. 7) were diverse, divided into periods (February-April, May-July, August-November, and December-January) that corresponded to eddy abundance patterns (Fig. 3A). CEs exhibit a mean monthly occurrence of 4.67 ± 0.29 active tracks, forming persistent, repeating vector loops that anchor over south-central depressions (MDT: -0.05 to -0.12 m) to define the highest-density footprints in the basin (>31 counts). ACEs stabilize as localized tracking clusters over southwestern and north-central open-ocean ridges (MDT: +0.14 to +0.22 m). Connecting these zones, compressed MDT gradients trace high-volume, margin-hugging corridors marked by maximum track line thickness along the southern continental slope and eastern shelf margins. During winter (DJF) and spring (MAM), active trajectories are tightly compressed along the immediate peripheral boundaries of the basin, driving tracking metrics to their annual maximums. In summer (JJA) and autumn (SON), features execute a significant offshore migration and spatial scattering into the open-ocean interior. This transition induces a steep decline in coastal track line thickness, reaching an absolute annual baseline minimum in July.

These patterns indicate that mesoscale eddies recur within persistent hotspots and along preferred transport pathways, with cyclonic eddies concentrated in high-density core regions and anticyclonic eddies occupying broader, lower-density areas that shift seasonally across the SEMS. These recurring patterns suggest that eddy formation and propagation are constrained by persistent circulation features and regional topography.

https://doi.org/10.5194/egusphere-2026-4744
Preprint. Discussion started: 21 August 2026


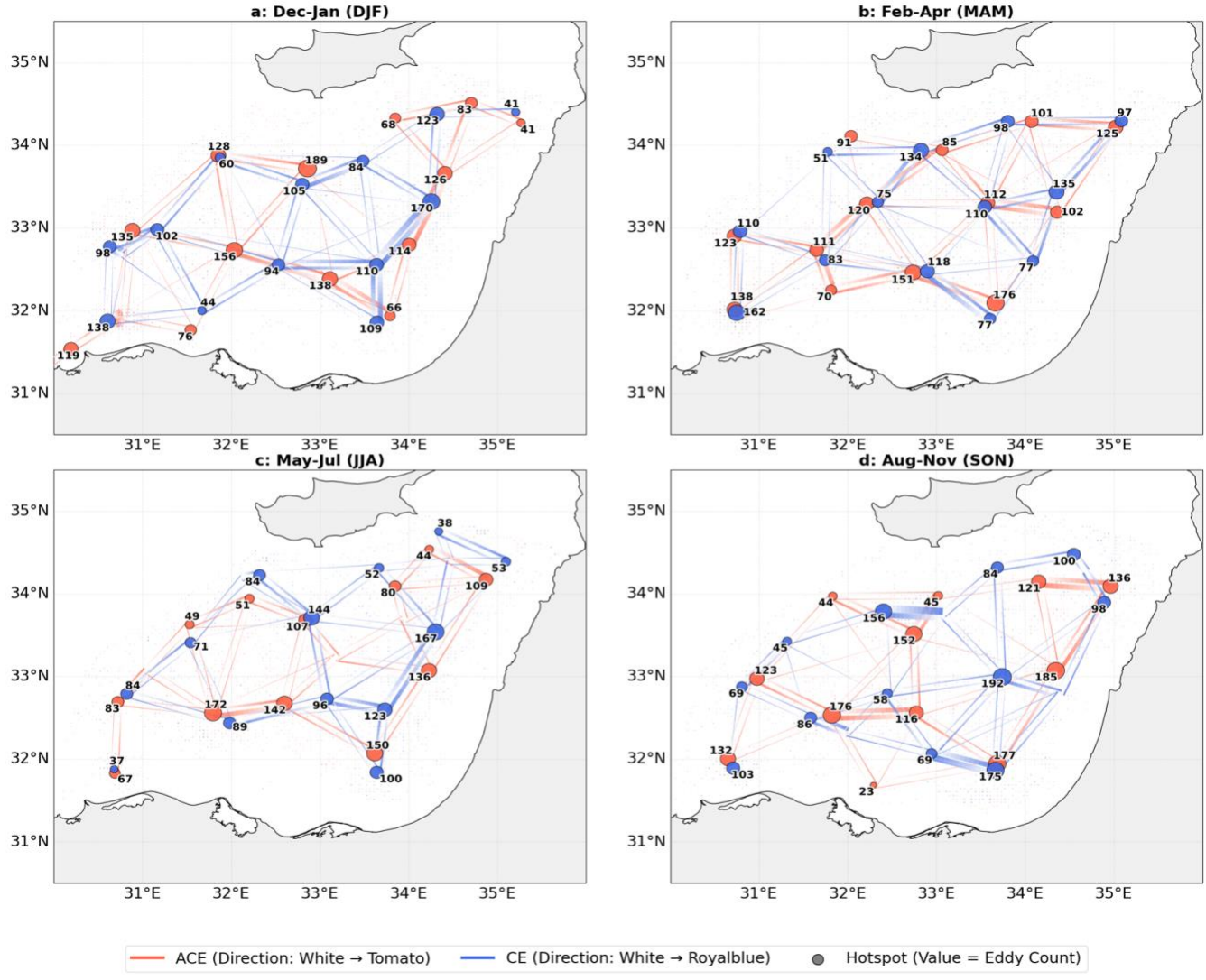


**Figure 7.** Seasonal directional flow and core hotspots of mesoscale eddies. This four-panel climatology illustrates the seasonal trajectories and aggregation centers of anticyclonic (ACE; red) and cyclonic (CE; blue) eddies in the Levantine Basin. Flow trajectories: Directional movement is indicated by a white-to-color gradient, where the white segments represent the point of origin and the solid color represents the terminal point of the eddy's seasonal track. Line thickness is scaled using a power-law relationship to emphasize high-volume "eddy corridors". Hotspots: Circles represent cluster centers where eddies frequently aggregate, with the area of the circle proportional to the cumulative seasonal count. Numerical labels within significant hotspots denote the exact number of unique eddy detections within that cluster. Background points represent individual daily significant locations. Mapping is performed on a 2x2 grid representing winter (**a**, DJF), spring (**b**, MAM), summer (**c**, JJA), and autumn (**d**, SON) periods.

https://doi.org/10.5194/egusphere-2026-4744
Preprint. Discussion started: 21 August 2026


## 4 Discussion

In this study, we analysed and compared two long-term datasets to characterize the spatial and seasonal variability of mesoscale eddy dynamics in the Southeastern Mediterranean Sea (SEMS), including eddy occurrence, radius, velocity, lifetime, and areas of influence. While cyclonic eddies (CEs) were generally more prevalent across the long-term datasets anticyclonic eddies (ACEs) were more persistent across the area (DYNED) and broader diffuse areas of influence at lower density counts. Furthermore, surface Chl *a* derived from satellite detections showed distinct seasonal co-variation with eddy dynamics, suggesting that eddies in the SEMS may be associated with changes in phytoplankton biomass through entrainment, retention, and redistribution of particles.
Although satellite-based measurements and discrete sampling hinder direct correlations with community responses (Anderson et al., 2021; Gronniger et al., 2023), this study highlights the potential links and emphasises the need for more coupled studies where physical and Chl *a* attributes in eddies are simultaneously investigated to improve our understanding of the functional role of eddies in ecosystem dynamics. This is especially important in the nutrient impoverished SEMS where environmental shifts are magnified by global change (Knobler et al., 2025; Ozer et al., 2022).

### 4.1 Eddy seasonality and area of influence (AOI)

Peaks in interannual eddy activity may be related to broader circulation changes in the southeastern Levantine Basin (Pujol and Larnicol, 2005), while the SEMS acts as a key eddy generation zone, playing a critical role in regional connectivity (Malauene et al., 2024; Mangolte et al., 2022; Oliveira et al., 2024; del Pilar Echeverri-García et al., 2022; Raya et al., 2025; Stuhlmacher and Gade, 2020). The spectral analysis suggested regional forcing mechanisms may modulate annual occurrences. This decadal-scale periodicity implies a potential coupling with broader basin-scale oscillations or intermittent circulation reversals characterizing the Eastern Mediterranean.

Our analysis suggests this region serves as a source for both CEs and ACEs, contributing to the transport of water masses and entrainment of biotic elements. The area of influence (AOI) of eddies may act as a measure of their ecosystem impact. CEs generally exhibit a denser AOI, consistently occupying a larger spatial extent within the highest-density zones compared to ACEs. While ACEs tend to be more prevalent regionally (Barboni et al., 2021; Mkhinini et al., 2014), recent high-resolution submesoscale observations show CEs are more numerous amongst smaller, shorter-lived features (Al-Darasi et al., 2025), whereas ACEs dominate among larger, longer-lived structures with stronger velocities.

During the summer oceanographic regime, strong stratification limits vertical mixing. Eddies are generally shallower, less vigorous, and largely confined to the upper 50 to 200 meters (Bonaduce et al., 2021). We observed a higher concentration of summer eddy occurrences along the southern and southeastern coastline of the SEMS, with a mean monthly CE occurrence reaching 4.67 ± 0.29. This suggests local bathymetric features, coastline configurations, or wind forcing patterns consistently influence eddy generation and movement in these areas.

https://doi.org/10.5194/egusphere-2026-4744
Preprint. Discussion started: 21 August 2026


During winter, weakened stratification and deep convective mixing allow eddies to penetrate deeper into the water column. Winter surface conditions (winds and waves) can diminish the surface signature of eddies, even while they maintain subsurface velocities up to 12.0 ± 0.6 cm $s^{-1}$ and mean radii up to 40.8 ± 0.9 km. Subsurface and double-core anticyclones significantly intensify winter mixed-layer deepening. When the winter mixed layer connects with a pre-existing subsurface anticyclonic core, it can lead to extreme mixed layer depth anomalies reaching depths of up to 300 meters (Barboni et al., 2021, 2023).

### 4.2 Negative Chl *a* anomaly in eddies and Chl *a* regimes

Our results for mean Chl *a* concentrations supported a seasonal dynamic, showing strong variability with peaks in late autumn and spring. CEs consistently maintain higher mean Chl *a* levels than ACEs, reaching the maximum values in early winter. While global paradigms traditionally characterize CEs as consistent productive oases driven by nutrient upwelling (Chelton et al., 2011; McGillicuddy, 2016), our finding that only ~23% of tracked SEMS eddies function as positive Chl *a* anomalies, and that these anomalies were restricted to specific combinations of eddy polarity, season, and lifetime, suggests that this binary model fails in ultraoligotrophic basins. Furthermore, unlike standard composite analyses that assume uniform core-centered productivity (Gaube et al., 2014; Kang et al., 2022), our high-resolution zonal analysis maps a dominant population of negative Chl *a* anomaly eddies with highly depleted cores.

While the statistical analyses confirmed that the four defined spatial zones are significantly different from one another, this variance did not indicate enhanced productivity. Most eddy features display a significant Chl *a* deficit relative to the background. This structural distinction is clearly illustrated by the internal gradient within the CE population where mean Chl *a* in the Core are depleted compared to both their immediate margins and more even to the ambient background waters.

The non-unimodal Chl *a* distribution within both the Core and Outer Ring suggest that CEs encompass a mixture of distinct Chl *a* regimes. This persists across all standard seasonal bins and life stages, masking the specific conditions required for true core enrichment, and challenges the static mesoscale frameworks applied to the SEMS by Belkin et al. (2022).

### 4.3 Surface footprint expansion and horizontal carrying capacity

Our long-term baseline documents a complete decoupling between localized surface Chl *a* concentrations and the total integrated surface footprint. While CEs yield higher localized peak concentrations, the integrated surface footprint is generally higher in ACEs. This footprint scales exponentially with the eddy radius ($R^2$), and thus the elevated signature within ACEs is mechanically driven by their larger physical dimensions and prolonged spatiotemporal persistence. The positive scaling observed between maximum rotational velocity and the integrated surface footprint provides direct physical evidence of fluid isolation. High peripheral orbital velocities form a closed kinematic boundary that physically traps the internal surface water mass, preventing cross-frontal dispersion. By trapping a vast horizontal area over extended lifecycles, ACEs dominate the transport and retention of specific surface-dwelling community assemblages (such as neuston and early-stage ichthyoplankton) and boundary-layer zooplankton across

https://doi.org/10.5194/egusphere-2026-4744
Preprint. Discussion started: 21 August 2026


the otherwise relatively poor Levantine Basin. Therefore, this integrated surface metric quantifies the horizontal carrying capacity of the surface boundary layer of the feature rather than total water-column production, serving primarily as a measure of surface processes impacting entrapment and entrainment.

### 4.4 Methodological constraints

From a methodological standpoint, it is critical to distinguish this 2D spatial integration from 3D volumetric biomass. Optical measurements of Chl *a* are inherently biased because other water column constituents specifically non-algal particles and coloured dissolved organic matter, interfere with light properties (Volpe et al., 2012) . This leads to inaccuracies in both the mean and integral Chl *a* concentrations, as well as estimations of biomass and carbon or nutrient flux. This bias is particularly pronounced in dynamic oceanic eddies where concentrations of mineral sediments, detritus, and dissolved organic matter vary significantly. Furthermore, recent profiling float studies demonstrate that surface Chl *a* anomalies often entirely misrepresent true 3D integrated biomass in oligotrophic regions where the Deep Chlorophyll Maximum (DCM) dominates (Cornec et al., 2021; Dufois et al., 2016). In the ultraoligotrophic SEMS, the true phytoplankton biomass peak sits permanently between 90 and 120 metres during stratified summer periods, acting as a physical barrier that prevents deeper nutrients from interacting with the surface layer (Lavigne et al., 2015; Yacobi et al., 1995). Because satellite-based optical sensors are limited to approximately the top 20 metres, substantial subsurface production layers remain largely undetected even in the oligotrophic SEMS.

Additionally, a portion of the statistical differences observed can be attributed to differences in detection algorithms rather than the physical ocean state, inherently distinguishing geometric from velocity-dynamical-based approaches. The multi-metric comparison between the AMEDA and py-eddy-tracker (PET) datasets reveals clear divergences in absolute values but strong agreement in low-frequency temporal patterns. The filter applied by the PET algorithm effectively ignores large-scale sea level fluctuations but might allow small-scale local changes in sea surface height to surpass the threshold for detection, capturing transient anomalies. It maintains the circular consistency of features but might end continuous tracking if surpassed, leading to shorter lifespans. This contrasts with velocity-based trackers like AMEDA that log continuous fluid coherence, demonstrating that eddy lifespans accepted in older literature may be partially skewed by geometric filter parameters rather than true physical termination.

### 4.5 Ecological implications and future work

The influence of mesoscale eddies on Chl *a* responses has been globally recognized. They affect water mass distribution and alter the vertical structure of the water column to weaken stratification, which boosts nutrient availability and alleviates nutrient limitations—a key factor in the P- and N-limited southeastern Mediterranean (Ben Ezra et al., 2021; Ozer et al., 2017). This can, in turn, enhance biomass and primary production (Clayton et al., 2013; Milliff and Robinson, 1992). Fluctuations in environmental conditions control the timing and magnitude of phytoplankton blooms bottom-up (Anderson et al., 2021), directly affecting subsequent zooplankton biomass and the broader food web (Mahadevan, 2014; Mahadevan et

https://doi.org/10.5194/egusphere-2026-4744
Preprint. Discussion started: 21 August 2026


al., 2012). Furthermore, specific eddy characteristics create localized pressures that increase selection and shape planktonic communities, retaining organisms for months across hundreds of kilometers (Condie and Condie, 2016).

Rather than acting solely as physical transport systems, our data suggests these mesoscale features fundamentally restructure the basal food web specifically the phytoplankton standing stock. The structural divergence we observed between cyclonic and anticyclonic features can be interpreted through the shifting balance of bottom-up nutrient fluxes and top-down grazing pressures, a dynamic that was previously observed in the SEMS by Belkin et al. (2022).

Our finding that CEs predominantly exhibit negative Chl *a* anomalies with heavily depleted cores structurally aligns with intense top-down regulation. While cyclonic upwelling traditionally introduces bottom-up nutrient fluxes into the euphotic zone, Belkin et al. (2022) demonstrated that SEMS cyclones can stimulate rapid micro- and mesozooplankton proliferation. This localized zooplankton enrichment exerts a severe top-down grazing pressure that actively strips out the phytoplankton standing stock. Consequently, the Chl *a* surplus is rapidly transferred to higher trophic levels rather than accumulating as surface pigment, directly yielding the suppressed, depleted Chl *a* signatures we observed at the cyclonic cores.

Conversely, the massive integrated phytoplankton footprints and winter anomaly spikes observed in ACEs highlight an ecological regime driven heavily by bottom-up processes. During periods of weakened stratification, deep convective mixing combined with the downwelling physical structure of anticyclones can trigger extreme mixed layer depths that alleviate intense nutrient limitations. Because these features may lack the intense, immediate top-down zooplankton grazing pressures associated with cyclonic cores, these bottom-up nutrient injections allow phytoplankton biomass to continuously accumulate (Belkin et al., 2022). Supported by extended lifespans (95 days) and massive spatial retention areas, ACEs serve as dominant, long-term horizontal carrying capacities for the phytoplankton communities in the SEMS.

Future studies should incorporate Lagrangian analyses to better assess how eddies affect marine life, focusing on both external transport (entrainment) and internal retention (trapping). While temporal variations in eddy dynamics and Chl *a* trends are strong, the spatial dynamics and specific mechanism such as the exact grazing rates within depletion zones, require further study, potentially integrating Lagrangian particle tracking, fine-scale biological sampling, and functional ecology models. Eddies function not merely as physical transport systems, but as active ecological agents shaping biogeographical patterns through dispersal limitation and environmental filtering (Clayton et al., 2013; Gronniger et al., 2023). As global climate change alters ocean circulation and stratification, understanding the role of mesoscale processes becomes increasingly important for predicting shifts in marine biodiversity and ecosystem function, especially in the SEMS, which can serve as a model system for global change.

https://doi.org/10.5194/egusphere-2026-4744
Preprint. Discussion started: 21 August 2026


## 5. Conclusions

The integration of long-term satellite datasets for mesoscale eddies and surface chlorophyll-a (Chl *a*) revealed that these features actively restructure the surface Chl *a* in the ultra-oligotrophic Southeastern Mediterranean Sea (SEMS). Rather than acting as passive transport mechanisms, eddies drive distinct ecological regimes based on polarity, seasonality and location. Cyclonic eddies (CEs) in the SEMS predominantly feature depleted surface Chl *a* cores. This structural depletion implies top-down biological regulation, where localized grazing pressure rapidly strips the phytoplankton standing stock. Anticyclonic eddies (ACEs) emerge as the primary ecological retainers within the basin. Their larger physical dimensions, extended lifespans, and strong kinematic boundaries facilitate integrated phytoplankton footprints via bottom-up accumulation. Less than a quarter of eddies had core-centric Chl *a* accumulation, Positive Chl *a* anomalies in ACEs peaked during winter while tightly compressed along the southeastern continental slope and eastern shelf margin, whereas CEs positive anomalies peak during autumn as they migrate offshore into the center of the SEMS.

## Appendix A

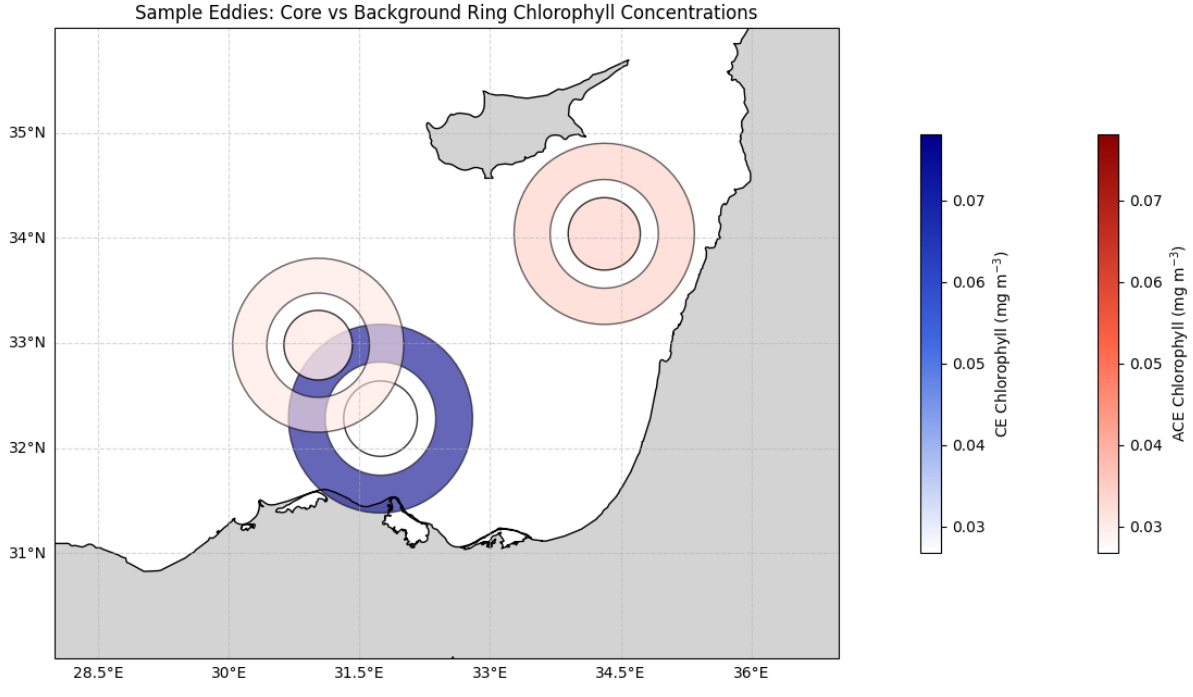


**Figure A1.** A schematic model of the the methodology used to evaluate the divergence between Chl *a* concentrations within the eddy core ($Chl_{in}$) and the ambient background environment ($Chl_{out}$). Internal (core) domain is delineated by the area enclosed within the maximum speed contour or the defined buffered radius (R). External (background) domain is defined as a concentric annular ring extending from

https://doi.org/10.5194/egusphere-2026-4744
Preprint. Discussion started: 21 August 2026


1.5×R to 2.5×R. This is intended to compute the Chl *a* anomaly (ΔChl) as the difference between internal Chl *a* levels and the reference background values. It should be noted that these eddies in scheme do not exist simultaneously.

## Code and data availability

The code used in this study is publicly available at https://github.com/Mrvy29/Eddy_Dynamics_OS26. All datasets used in the analyses are available through open-access repositories, including the Copernicus Data Store, the DYNED Atlas (https://www.lmd.polytechnique.fr/dyned/), and the Meta3.2 NRT (Aviso) Atlas (https://www.aviso.altimetry.fr/en/data/products/value-added-products/global-mesoscale-eddy-trajectory-product/meta3-2-exp-nrt.html).

## Author contributions

Funding acquisition: TGH and AL. Conceptualization and methodology: TGH, AL and MG. Analyses: MG. Data processing: MG. Formal analysis: MG with interactions from all co-authors. Preparation and writing of the manuscript: MG with contributions from all co-authors.

## Competing interests

The authors declare no competing interests.

## Acknowledgements

We would like to thank the Israel Oceanographic and Limnological Research (IOLR), the University of Haifa and the Helmholtz funded International Laboratory; The Eastern Mediterranean Sea Center- An Early-Warning Model-System for our Future Oceans: EMS Future Ocean Research (EMS FORE); the Tzvi Keinan fund for funding for supporting M. Gilboa's scholarship. This study is in partial fulfilment of the PhD requirements for M. Gilboa at the Leon H. Charney School of Marine Sciences, at the University of Haifa.

## Financial support

This research was supported by the Israel Ministry of Science and Technology grant no. 2030 to T. Guy-Haim and A. Lazar. This project was supported in part by the Israel Science Foundation (ISF) [grant number 1666/18].

https://doi.org/10.5194/egusphere-2026-4744
Preprint. Discussion started: 21 August 2026


## References

Al-Darasi, M., Li, Z., Wu, W., Muallem, E., Taqi, A., and Zhang, X.: Exploring mesoscale eddies in the Mediterranean: A remote sensing approach with META3 product data, J. Coast. Res., 41, 482–495, 2025.

Anderson, S. I., Barton, A. D., Clayton, S., Dutkiewicz, S., and Rynearson, T. A.: Marine phytoplankton functional types exhibit diverse responses to thermal change, Nat. Commun., 12, 6413, 2021.

Barboni, A., Lazar, A., Stegner, A., and Moschos, E.: Lagrangian eddy tracking reveals the Eratosthenes anticyclonic attractor in the eastern Levantine Basin, Ocean Sci., 17, 1231–1250, 2021.

Barboni, A., Coadou-Chaventon, S., Stegner, A., Le Vu, B., and Dumas, F.: How subsurface and double-core anticyclones intensify the winter mixed-layer deepening in the Mediterranean Sea, Ocean Sci., 19, 229–250, 2023.

Belkin, N., Guy-Haim, T., Rubin-Blum, M., Lazar, A., Sisma-Ventura, G., Kiko, R., Morov, A. R., Ozer, T., Gertman, I., Herut, B., and Rahav, E.: Influence of cyclonic and anticyclonic eddies on plankton in the southeastern Mediterranean Sea during late summertime, Ocean Science, 18, https://doi.org/10.5194/os-18-693-20, 2022.

Ben Ezra, T., Krom, M. D., Tsemel, A., Berman-Frank, I., Herut, B., Lehahn, Y., Rahav, E., Reich, T., Thingstad, T. F., and Sher, D.: Seasonal nutrient dynamics in the P depleted Eastern Mediterranean Sea, Deep Sea Res. Part 1 Oceanogr. Res. Pap., 176, 103607, 2021.

Bonaduce, A., Cipollone, A., Johannessen, J. A., Staneva, J., Raj, R. P., and Aydogdu, A.: Ocean Mesoscale Variability: A Case Study on the Mediterranean Sea From a Re-Analysis Perspective, Front Earth Sci. Chin., 9, https://doi.org/10.3389/feart.2021.724879, 2021.

Cael, B. B., Bisson, K., Boss, E., and Liu, Z.: Surface ocean chlorophyll: Do the Green get greener and the blue bluer?, Geophys. Res. Lett., 53, e2025GL120527, 2026.

Chelton, D. B., Gaube, P., Schlax, M. G., Early, J. J., and Samelson, R. M.: The influence of nonlinear mesoscale eddies on near-surface oceanic chlorophyll, Science, 334, 328–332, 2011.

Clayton, S., Dutkiewicz, S., Jahn, O., and Follows, M. J.: Dispersal, eddies, and the diversity of marine phytoplankton, Limnol. Oceanogr., 3, 182–197, 2013.

Condie, S. and Condie, R.: Retention of plankton within ocean eddies: Retention in ocean eddies, Glob. Ecol. Biogeogr., 25, 1264–1277, 2016.

Cornec, M., Laxenaire, R., Speich, S., and Claustre, H.: Impact of mesoscale eddies on deep Chlorophyll Maxima, Geophys. Res. Lett., 48, e2021GL093470, 2021.

https://doi.org/10.5194/egusphere-2026-4744
Preprint. Discussion started: 21 August 2026


Dufois, F., Hardman-Mountford, N. J., Greenwood, J., Richardson, A. J., Feng, M., and Matear, R. J.: Anticyclonic eddies are more productive than cyclonic eddies in subtropical gyres because of winter mixing, Sci Adv, 2, e1600282, 2016.

Eusebi Borzelli, G. L. and Carniel, S.: A reconciling vision of the Adriatic-Ionian Bimodal Oscillating System, Sci. Rep., 13, 2334, 2023.

Fadida, Y., Ozer, T., Ben Ezra, T., Krom, M. D., Tsemel, A., Tsagaraki, T. M., Biton, E., Toledo, Y., and Lehahn, Y.: Coastal eddies as vectors for connectivity during the summer in the Levantine sea, , https://doi.org/10.5194/egusphere-2026-1507, 2026.

Gačić, M., Schroeder, K., Civitarese, G., Cosoli, S., Vetrano, A., and Eusebi Borzelli, G. L.: Salinity in the Sicily Channel corroborates the role of the Adriatic–Ionian Bimodal Oscillating System (BiOS) in shaping the decadal variability of the Mediterranean overturning circulation, Ocean Sci., 9, 83–90, 2013.

Gaube, P., McGillicuddy, D. J., Jr, Chelton, D. B., Behrenfeld, M. J., and Strutton, P. G.: Regional variations in the influence of mesoscale eddies on near-surface chlorophyll, J. Geophys. Res. C: Oceans, 119, 8195–8220, 2014.

Graser, A. and Dragaschnig, M.: Open geospatial tools for movement data exploration, KN J. Cartogr. Geogr. Inf., 70, 3–10, 2020.

Gronniger, J. L., Gray, P. C., Niebergall, A. K., Johnson, Z. I., and Hunt, D. E.: A Gulf Stream frontal eddy harbors a distinct microbiome compared to adjacent waters, bioRxiv, https://doi.org/10.1101/2023.02.23.529726, 2023.

Kang, J., Wang, Y., Huang, S., Pei, L., and Luo, Z.: Impacts of mesoscale eddies on biogeochemical variables in the northwest Pacific, J. Mar. Sci. Eng., 10, 1451, 2022.

Knobler, S., Rilov, G., Garfinkel, C. I., and Liberzon, D.: Climate change impacts in Eastern Mediterranean Sea: Trends and extremes, Water Waves, 7, 521–556, 2025.

Lavigne, H., D'Ortenzio, F., Ribera D'Alcalà, M., Claustre, H., Sauzède, R., and Gacic, M.: On the vertical distribution of the chlorophyll *a* concentration in the Mediterranean Sea: a basin-scale and seasonal approach, Biogeosciences, 12, 5021–5039, 2015.

Mahadevan, A.: Ocean science: eddy effects on biogeochemistry: Ocean science, Nature, 506, 168–169, 2014.

Mahadevan, A., D'Asaro, E., Lee, C., and Perry, M. J.: Eddy-Driven Stratification Initiates North Atlantic Spring Phytoplankton Blooms, Science, 337, 54 LP – 58, 2012.

Malauene, B. S., Lett, C., Marsac, F., Penven, P., Abdula, S., Moloney, C. L., and Roberts, M. J.: Influence of Mozambique Channel eddies on larval loss of two shallow-water commercial shrimp species, PLOS Clim, 3, e0000414, 2024.

https://doi.org/10.5194/egusphere-2026-4744
Preprint. Discussion started: 21 August 2026


Mangolte, I., Lévy, M., Dutkiewicz, S., Clayton, S., and Jahn, O.: Plankton community response to fronts: winners and losers, J. Plankton Res., 44, 241–258, 2022.

McGillicuddy, D. J., Jr: Mechanisms of physical-biological-biogeochemical interaction at the oceanic mesoscale, Ann. Rev. Mar. Sci., 8, 125–159, 2016.

Milliff, R. F. and Robinson, A. R.: Structure and dynamics of the Rhodes gyre system and dynamical interpolation for estimates of the mesoscale variability, J. Phys. Oceanogr., 22, 317–337, 1992.

Mkhinini, N., Coimbra, A. L. S., Stegner, A., Arsouze, T., Taupier-Letage, I., and Béranger, K.: Long-lived mesoscale eddies in the eastern Mediterranean Sea: Analysis of 20 years of AVISO geostrophic velocities, J. Geophys. Res. C: Oceans, 119, 8603–8626, 2014.

Oliveira, G. F., Pimentel-Santos, J., Gomes, I., Albuquerque, R., Queiroga, H., and Peteiro, L. G.: Seasonal and synoptic spatio-temporal variability on larval delivery mechanisms inferred from mussel settlement patterns in the Portuguese coast, Estuar. Coast. Shelf Sci., 305, 108875, 2024.

Ozer, T., Gertman, I., Kress, N., Silverman, J., and Herut, B.: Interannual thermohaline (1979–2014) and nutrient (2002–2014) dynamics in the Levantine surface and intermediate water masses, SE Mediterranean Sea, Glob. Planet. Change, 151, 60–67, 2017.

Ozer, T., Rahav, E., Gertman, I., Sisma-Ventura, G., Silverman, J., and Herut, B.: Relationship between thermohaline and biochemical patterns in the levantine upper and intermediate water masses, Southeastern Mediterranean Sea (2013–2021), Front. Mar. Sci., 9, https://doi.org/10.3389/fmars.2022.958924, 2022.

Pegliasco, C., Delepoulle, A., Mason, E., Morrow, R., Faugère, Y., and Dibarboure, G.: META3.1exp: a new global mesoscale eddy trajectory atlas derived from altimetry, Earth Syst. Sci. Data, 14, 1087–1107, 2022.

del Pilar Echeverri-García, L., Daudén-Bengoa, G., Compaire, J. C., Jiménez-Rosenberg, S. P. A., Pérez-Brunius, P., Ferreira-Bartrina, V., and Herzka, S. Z.: Variability of fish larvae assemblages relative to mesoscale features in the deep water region of the southern Gulf of Mexico, Hydrobiologia, 849, 1471–1493, 2022.

Pujol, M.-I. and Larnicol, G.: Mediterranean sea eddy kinetic energy variability from 11 years of altimetric data, J. Mar. Syst., 58, 121–142, 2005.

Raya, V., Olivar, M. P., Salat, J., Mir-Arguimbau, J., Guerrero, E., and Sabatés, A.: Variability of larval fish assemblages under contrasting winter environmental conditions in the northwestern Mediterranean sea, Mar. Environ. Res., 205, 107025, 2025.

Stegner, A. and Le Vu, B.: Atlas of 3D eddies in the Mediterranean sea, https://doi.org/10.24400/527896/A01-2022.014, 2022.

https://doi.org/10.5194/egusphere-2026-4744
Preprint. Discussion started: 21 August 2026


678 Stuhlmacher, A. and Gade, M.: Statistical analyses of eddies in the Western Mediterranean Sea based
679 on Synthetic Aperture Radar imagery, Remote Sens. Environ., 250, 112023, 2020.

680 Tanaka, T., Zohary, T., Krom, M. D., Law, C. S., Pitta, P., Psarra, S., Rassoulzadegan, F., Thingstad, T.
681 F., Tselepides, A., Woodward, E. M. S., Flaten, G. A. F., Skjoldal, E. F., and Zodiatis, G.: Microbial
682 community structure and function in the Levantine Basin of the eastern Mediterranean, Deep Sea Res.
683 Part I, 54, 1721–1743, 2007.

684 Teruzzi, A., Di Biagio, V., Feudale, L., Bolzon, G., Lazzari, P., Salon, S., Coidessa, G., and Cossarini,
685 G.: Mediterranean Sea Biogeochemical Reanalysis (CMEMS MED-Biogeochemistry, MedBFM3
686 system) (Version 1), 2021.

687 Volpe, G., Colella, S., Forneris, V., Tronconi, C., and Santoleri, R.: The Mediterranean Ocean Colour
688 Observing System – system development and product validation, Ocean Sci., 8, 869–883, 2012.

689 Yacobi, Y. Z., Zohary, T., Kress, N., Hecht, A., Robarts, R. D., Waiser, M., Wood, A. M., and Li, W.
690 K. W.: Chlorophyll distribution throughout the southeastern Mediterranean in relation to the physical
691 structure of the water mass, J. Mar. Syst., 6, 179–190, 1995.

692 Zhao, D., Xu, Y., Zhang, X., and Huang, C.: Global chlorophyll distribution induced by mesoscale
693 eddies, Remote Sens. Environ., 254, Not Available, 2022.

694